



Structural coordination of polymerization and crosslinking by a SEDS–bPBP peptidoglycan synthase complex

Megan Sjodt¹, Patricia D. A. Rohs², Morgan S. A. Gilman¹, Sarah C. Erlandson¹, Sanduo Zheng¹, Anna G. Green³, Kelly P. Brock³ , Atsushi Taguchi² , Daniel Kahne⁴, Suzanne Walker² , Debora S. Marks³, David Z. Rudner², Thomas G. Bernhardt^{2,5}  and Andrew C. Kruse¹  

The shape, elongation, division and sporulation (SEDS) proteins are a highly conserved family of transmembrane glycosyltransferases that work in concert with class B penicillin-binding proteins (bPBPs) to build the bacterial peptidoglycan cell wall^{1–6}. How these proteins coordinate polymerization of new glycan strands with their crosslinking to the existing peptidoglycan meshwork is unclear. Here, we report the crystal structure of the prototypical SEDS protein RodA from *Thermus thermophilus* in complex with its cognate bPBP at 3.3 Å resolution. The structure reveals a 1:1 stoichiometric complex with two extensive interaction interfaces between the proteins: one in the membrane plane and the other at the extracytoplasmic surface. When in complex with a bPBP, RodA shows an approximately 10 Å shift of transmembrane helix 7 that exposes a large membrane-accessible cavity. Negative-stain electron microscopy reveals that the complex can adopt a variety of different conformations. These data define the bPBP pedestal domain as the key allosteric activator of RodA both *in vitro* and *in vivo*, explaining how a SEDS–bPBP complex can coordinate its dual enzymatic activities of peptidoglycan polymerization and crosslinking to build the cell wall.

The peptidoglycan cell wall defines bacterial cell shape and maintains cellular integrity. Inhibiting the synthesis of the cell wall is among the most effective strategies for treating bacterial infections^{7,8}. Peptidoglycan biogenesis begins inside the cell on the inner leaflet of the plasma membrane, where the lipid-linked disaccharide-pentapeptide precursor molecule lipid II is synthesized and then translocated to the extracellular membrane surface by the lipid II flippase MurJ^{9,10}. Synthesis of peptidoglycan from lipid II requires two enzymatic activities. First, peptidoglycan glycosyltransferase enzymes polymerize long glycan strands from the disaccharide headgroup of lipid II. Second, polymerized glycans are crosslinked into the existing cell wall through their peptides by transpeptidase enzymes. Class A penicillin-binding proteins (PBPs) contain both the glycosyltransferase and transpeptidase domains in a single polypeptide; for many years, these and related monofunctional enzymes were the only known cell wall polymerases. However, it has recently been shown that integral membrane proteins of the shape, elongation, division and sporulation (SEDS) family comprise a second class of peptidoglycan polymerases capable of working in concert

with class B PBPs (bPBPs) to both polymerize and crosslink peptidoglycan. Thus, the SEDS–bPBP complex constitutes a peptidoglycan synthase machine that recapitulates the bifunctionality of class A PBPs in two separate polypeptides^{1–5} (Fig. 1a). SEDS–bPBP systems are more widely conserved than class A PBPs, although commonly both systems are present and function in parallel to facilitate cell wall synthesis^{1,9}. In view of its essential role in peptidoglycan biogenesis, the SEDS–bPBP complex is an attractive target for therapeutic design to combat the rise of antibiotic resistance in pathogenic bacteria.

Previously, we solved the structure of the prototypical SEDS protein family member RodA from *Thermus thermophilus* and predicted the interface between ^{Ti}RodA and its cognate bPBP (^{Ti}PBP2) using evolutionary coupling analysis¹¹. These data in combination with recent genetic and biochemical studies^{4,5} strongly indicate that RodA and PBP2 function as a complex *in vivo*. To better understand how these two proteins work together, we sought to characterize their interaction in molecular detail through a combination of biochemical and crystallographic methods.

RodA and PBP2 from *T. thermophilus* were co-expressed and purified, resulting in a stoichiometric complex (Supplementary Fig. 1). The complex was then crystallized by the lipidic cubic phase method (Supplementary Fig. 1) (ref. ¹²); X-ray diffraction datasets were collected to resolutions of 3.5 and 3.3 Å for a wild-type (WT) complex and a catalytically inactive RodA^{D255A} variant complex treated with ampicillin, respectively (Supplementary Table 1). The structures of WT RodA and D255A variant complexes were virtually identical, so we focused on the modestly higher resolution RodA^{D255A}–PBP2 structure. The ^{Ti}RodA–PBP2 complex adopts a surprisingly compact conformation where RodA and the transmembrane segment of PBP2 lie within the membrane plane, while the pedestal domain of PBP2 sits on top of the extracytoplasmic loops of RodA (Fig. 1b). The structure of the ^{Ti}PBP2 ectodomain shares the same overall domain architecture as the PBP2 proteins of *Helicobacter pylori* and *Escherichia coli* (Supplementary Figs 2 and 3) (refs. ^{13,14}). The N-terminal transmembrane domain is connected by a short hinge region to the pedestal domain, which is formed by two subdomains—the anchor and head subdomains. The anchor is composed of a small β-sheet formed by the β1 strand and β8–β9 hairpin and is connected to the hinge region by an extensive

¹Department of Biological Chemistry and Molecular Pharmacology, Blavatnik Institute, Harvard Medical School, Boston, MA, USA. ²Department of Microbiology, Blavatnik Institute, Harvard Medical School, Boston, MA, USA. ³Department of Systems Biology, Blavatnik Institute, Harvard Medical School, Boston, MA, USA. ⁴Department of Chemistry and Chemical Biology, Harvard University, Cambridge, MA, USA. ⁵Howard Hughes Medical Institute, Chevy Chase, MD, USA. ✉e-mail: andrew_kruse@hms.harvard.edu

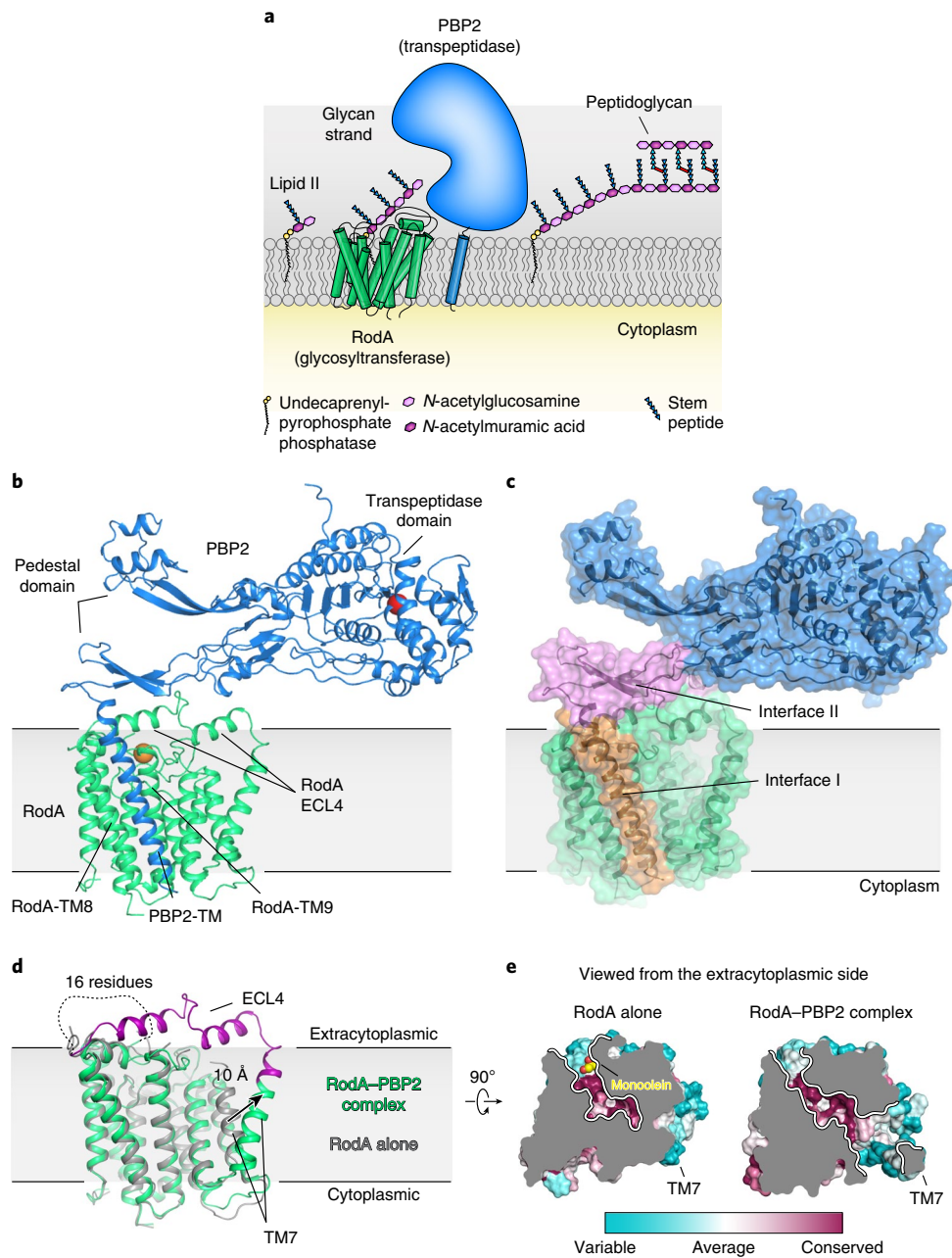


Fig. 1 | Crystal structure of the *T. thermophilus* RodA-PBP2 peptidoglycan synthase complex. **a, RodA polymerizes glycans strands from lipid II precursor molecules and PBP2 crosslinks the newly formed glycans to the existing peptidoglycan cell wall. **b**, Structure of the RodA-PBP2 complex viewed parallel to the membrane plane. The active site residue (Ser308) in the transpeptidase domain of PBP2 and Asp255 in RodA are shown as red and orange spheres, respectively. A short peptide that was modelled in the pedestal domain was removed for clarity. **c**, Surface view showing two distinct interfaces. Interface I (orange) is within the membrane plane, while interface II (pink) lies above the membrane. **d**, Comparison of the structure of RodA in isolation (PDB code: 6BAR; grey) and RodA in complex with PBP2 (green). Newly resolved residues in ECL4 of RodA in the PBP2 complex are highlighted in purple. **e**, Top-down surface view cross-section of the highly conserved membrane-accessible cavities in both RodA structures.**

network of hydrogen bonds and salt bridges (Supplementary Fig. 2). This is followed by the head domain, which is composed of a small discontinuous β -sheet, with four interspersed α -helices that form the remainder of the head subdomain, as well as the linker subdomain connecting the pedestal and transpeptidase domains. The C-terminal transpeptidase domain possesses the common penicillin-binding protein fold and a core β -sheet surrounded by α -helices; it lies just above the membrane plane, positioned approximately 80 Å away from central core of RodA. Although the structure of each subdomain is well conserved between *T. thermophilus* and the PBP2

proteins of other species, the relative orientation of these domains differs in each of the determined structures (Supplementary Fig. 2).

There are two main interprotein interfaces in the RodA-PBP2 complex structure (Fig. 1c). The first lies within the membrane plane where the transmembrane domain of PBP2 packs tightly against transmembrane 8 (TM8) and 9 (TM9) of RodA. This interface is almost entirely hydrophobic and seems to be driven by steric compatibility (Extended Data Fig. 1)¹⁵. It agrees well with our previously predicted interaction interface¹¹ (Extended Data Fig. 2) as well as predictions of the *E. coli* FtsW-FtsI interface by others^{5,16},

both of which were identified using evolution sequence covariation methods¹⁷. A second interface lies above the membrane plane and is exposed to the extracytoplasmic environment where a three-stranded β -sheet within the pedestal domain of PBP2 (residues Glu30–Ala50 and Lys181–Thr205) as well as a small helical loop (residues Asn151–Ser160) lie on top of RodA's extracellular loop 4 (ECL4, residues Pro189–Gly232), which was partially disordered in the previously determined structure of RodA¹¹. The previously unresolved residues form two α -helices connected by a short, ordered loop (Fig. 1d), albeit with elevated B-factors relative to the overall complex suggesting it is either conformationally heterogeneous or mobile. The density for the remaining 16 residues (Leu233–Phe248) was too poor to model, suggesting that these residues are still partially disordered in the crystal. Most contacts at interface II are between α -helix 10 in RodA ECL4 and the pedestal domain of PBP2 (Extended Data Fig. 3). However, very few specific interactions are present in this interface, suggesting that interface I provides most of the energy required for the binding of RodA and PBP2.

The overall structure of RodA in the complex remains largely unchanged from the structure of RodA in isolation (C α root mean square deviation (RMSD) = 0.5 Å; Protein Data Bank (PDB) code: 6BAR) with the exception of a very large outward deflection of transmembrane 7 (TM7) by approximately 10 Å. TM7 directly precedes ECL4; in the more ordered configuration adopted in the presence of PBP2, the N-terminal portion of ECL4 is oriented away from the core of RodA and appears to drag the C-terminal region of TM7 outwards, resulting in an observed tilt of TM7 by approximately 20°. Intriguingly, the shift in TM7 exposes a large membrane-accessible cavity that was occluded in the structure of RodA alone (Fig. 1e and Extended Data Fig. 4). This cavity is approximately 15 Å wide by approximately 30 Å tall and is large enough to accommodate a lipid II molecule; therefore, it could be a substrate entry or exit site.

Previous studies on SED–bPBP complexes in *E. coli* and *Streptococcus thermophilus* have shown that bPBPs allosterically stimulate SEDS glycosyltransferase activity in vitro⁴⁵. Therefore, we tested whether *T. thermophilus* PBP2 could also activate RodA. Indeed, peptidoglycan polymers were produced only when both RodA and PBP2 were present in the reaction, and there was no detectable glycosyltransferase activity by either RodA or PBP2 alone (Fig. 2a,b). Moreover, the glycosyltransferase activity of RodA increased as sub-stoichiometric amounts of PBP2 were added and reached a plateau on addition of an equimolar amount of PBP2, in agreement with the 1:1 stoichiometry observed in the crystal structure. The RodA–PBP2 extracytoplasmic interface II seen in our structure includes a large portion of ECL4 of RodA, which was disordered in the structure of RodA alone¹¹. Since ECL4 contains residues that are essential for the function of RodA¹, including residues equivalent to Gln200 and Asp255, we hypothesized that the pedestal domain of PBP2 might function in allosteric activation of RodA in part by stabilizing a catalytically competent conformation of ECL4. This would serve to license peptidoglycan polymerization only when a bPBP is present to crosslink resulting glycan strands, thereby avoiding futile consumption of lipid II (ref. 18).

To test this hypothesis, we introduced amino acid substitutions in the PBP2 pedestal domain at the interface with the RodA ECL4 and tested their effect on WT RodA glycosyltransferase activity in vitro (Fig. 2c). We sought to disrupt this interface by mutating hydrophobic residues on β 1 and β 6 of PBP2 to arginine to introduce a bulky, charged side chain in the centre of this binding interface (Extended Data Fig. 3). As shown in Fig. 2d, glycosyltransferase activity was reduced when an arginine residue was introduced at residue Leu43 or Ala186 within the PBP2 pedestal domain (PBP2^{L43R} and PBP2^{A186R}). These PBP2 variants still efficiently copurified with RodA (Extended Data Fig. 5), suggesting that while they can still form a complex with RodA they are impaired in their ability to promote its glycosyltransferase activity.

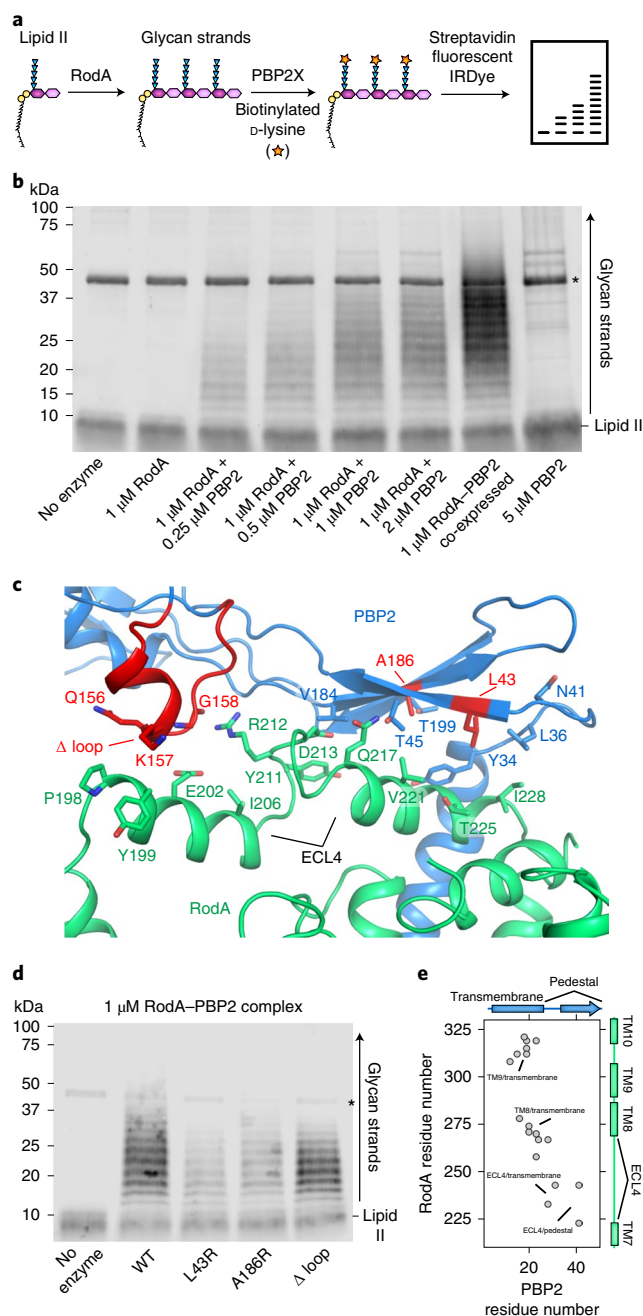


Fig. 2 | PBP2 activates RodA glycosyltransferase activity through its pedestal domain. **a**, Graphical representation of the polyacrylamide gel-based assay to detect RodA glycosyltransferase activity in vitro. The terminal residues in the stem peptide of the polymerized glycan strands and the lipid II precursor are exchanged with biotinylated D-lysine via *E. faecalis* PBP2X transpeptidase enzyme, transferred to a polyvinylidene fluoride membrane and then detected by fluorescently labelled streptavidin (IRDye 800CW streptavidin). **b**, RodA polymerizes lipid II only in the presence of PBP2. The asterisk represents the PBP2X biotinylating enzyme. Note that complexes purified following co-expression are more active than when they are reconstituted from individual preparations. Representative image of one of three experiments. **c**, Close-up view of RodA–PBP2 extracytoplasmic interface II. Amino acid substitutions are indicated in red. **d**, Substitutions in the PBP2 pedestal domain impair RodA glycosyltransferase activity in vitro. The asterisk represents the PBP2X biotinylating enzyme. Representative image of one of two experiments. **e**, Evolutionary covariation map showing 19 evolutionary couplings between RodA and PBP2, generated from previously published data¹¹.

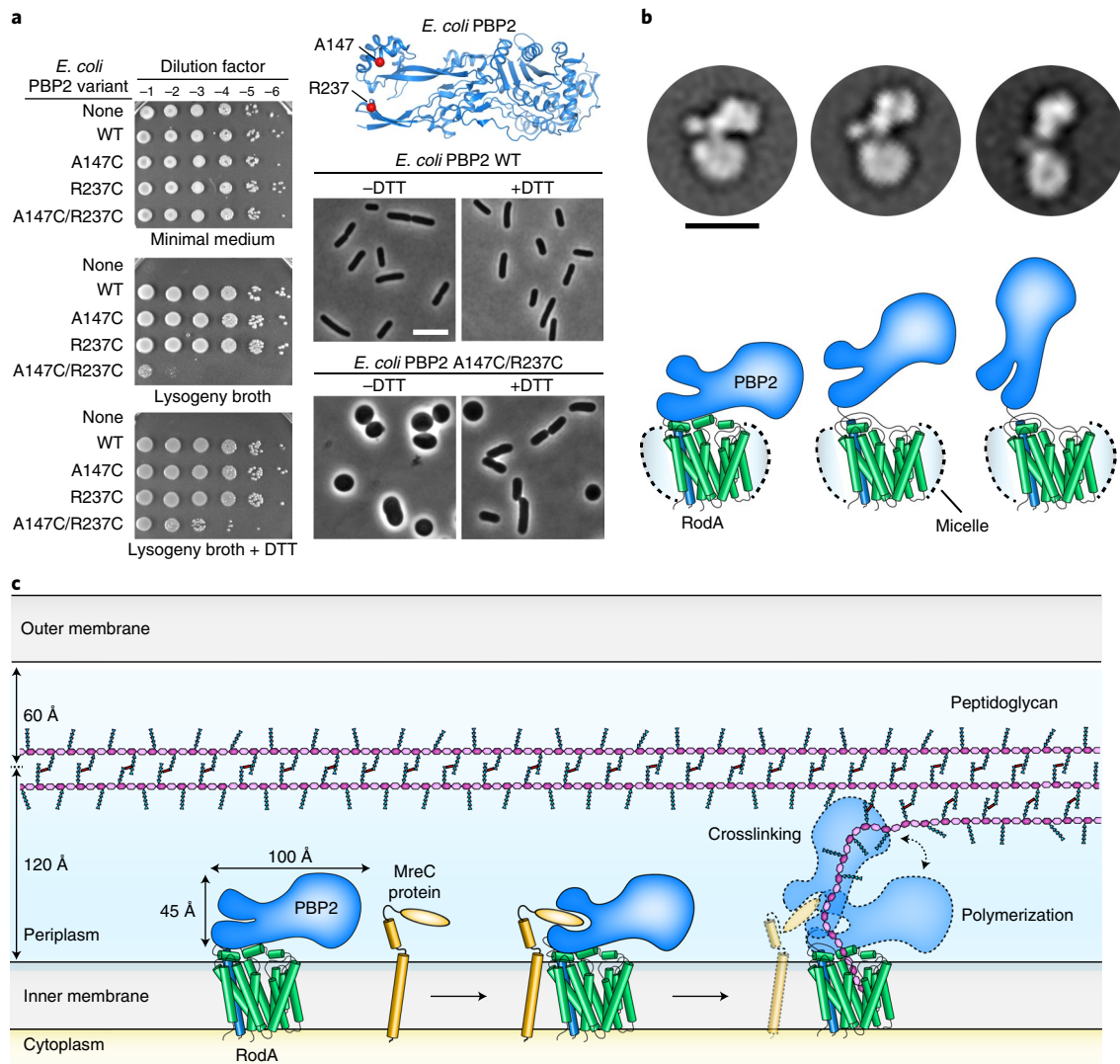


Fig. 3 | The RodA-PBP2 complex adopts a broad range of conformations to facilitate cell wall synthesis. **a**, Locking the pedestal domain of PBP2 is lethal in *E. coli*. The top right panel shows the *E. coli* PBP2 structure¹³ (PDB code: 6G9P), highlighting the cysteine substitutions as red spheres. Overnight cultures of the *E. coli* strains where RodA-PBP2 had been deleted and complemented with a plasmid encoding RodA without PBP2 ('None') or RodA with the PBP2 variants listed were serially diluted and spotted on either M9 minimal medium agar (Rod non-essential) or lysogeny broth agar (Rod essential) in the presence or absence of 10 mM DTT (left panel). The bottom right panels show micrographs of *E. coli* cells inactivated for native PBP2 expressing either PBP2 (WT) or the cysteine variant from a plasmid. Scale bar, 5 μ m. Results shown are derived from one experiment with $n=650$ cells analysed per group but are representative of two experiments. **b**, Representative negative-stain electron microscopy 2D class averages of the RodA-PBP2 complex (top panel) depicting different conformations, which are schematically represented in the bottom panel. The images were collected on a Tecnai T12 microscope and the resulting class averages were calculated from a total of 32,152 particles. Scale bar, 10 nm. **c**, Model of RodA-PBP2-mediated peptidoglycan cell wall synthesis. The dimensions of the RodA-PBP2 complex structure are shown in relation to the Gram-negative bacterial cell envelope.

Interestingly, RodA glycosyltransferase activity was largely maintained when residues Ala150-Pro161 were deleted from PBP2 (PBP2^{Δ100P}), indicating that this region does not play a major role in activating RodA or stimulating RodA activity. This result is not entirely surprising since the evolutionary couplings between RodA and PBP2 were mainly localized to the transmembrane of PBP2 and the N-terminal region of the pedestal domain (Fig. 2e)¹¹, indicating that these regions are subject to stronger evolutionary selection pressure than the Ala150-Pro161 loop. Taken together with the evolutionary couplings, our results suggest that the PBP2 pedestal domain is critical for stimulating RodA glycosyltransferase activity. This is consistent with previous data suggesting a similar role for the pedestal domain of PBP2a of *Staphylococcus aureus*, suggesting that this may be a common feature of bPBPs¹⁹.

In view of the importance of the PBP2 pedestal domain, it is interesting to note that this region is also important for interactions with another Rod system protein, MreC, which is essential in vivo. Although the effect of MreC in vitro has not yet been measured, amino acid substitutions in MreC can be rescued by compensatory substitutions in either RodA or PBP2 (ref. 4). Interestingly, these same substitutions in RodA-PBP2 result in higher glycosyltransferase activity than WT controls, suggesting that MreC functions normally by stimulating RodA glycosyltransferase activity. This protein may promote RodA glycosyltransferase activity through interactions with the pedestal domain of PBP2 (ref. 4). In our structure of the RodA-PBP2 complex, the pedestal domain of PBP2 adopts an open V-shaped architecture reminiscent of MreC-bound PBP2 (ref. 14) (Extended Data Fig. 6). To test if pedestal domain opening

is important for RodA activity *in vivo*, we introduced two cysteine substitutions in PBP2 that could form a disulfide bond if the pedestal adopts a closed conformation like the one observed in the *H. pylori* PBP2 structure without MreC¹⁴. For these studies, we used the *E. coli* PBP2 (*Ec*PBP2) so that the effects of these variants could be measured *in vivo*. As described earlier (Supplementary Fig. 2), the structure of the *T. thermophilus* PBP2 is highly similar to the PBP2 of both *E. coli* and *H. pylori*, indicating that the structural features observed in *T. thermophilus* probably translate well to other organisms. At the time, the structure of *E. coli* PBP2 had not yet been published and the *H. pylori* PBP2 structure was used to design these variants.

E. coli cells where the *pbpA-rodA* locus had been deleted were transformed with vectors encoding RodA and different variants of PBP2. These cells were capable of growth on minimal media, on which the Rod system is not required, but could only grow on lysogeny broth media when RodA and PBP2 were complemented, consistent with the long-standing observation that the Rod system is required for growth on lysogeny broth (Fig. 3a). Strains harbouring the double cysteine substitution (*Ec*PBP2^{A147C/R237C}) were impaired in their ability to grow on lysogeny broth and displayed severe morphological defects. Quantification of the cell morphologies revealed a significantly different aspect ratio for WT and *Ec*PBP2^{A147C/R237C} cells (3.58 ± 0.77 and 1.47 ± 0.58 , respectively for $n=650$ cells). These effects were partially rescued by adding the reducing agent dithiothreitol (DTT) to the growth medium, with a corresponding increase in aspect ratio only for the mutant cells (3.38 ± 0.83 and 2.54 ± 1.2 , for WT and mutant cells, respectively in the presence of DTT, $n=650$). Importantly, these PBP2 variants retained the ability to copurify with RodA, indicating that these defects are not the result of reduced binding to RodA (Extended Data Fig. 7). Given that similar disulfide locking of *H. pylori* PBP2 reduces binding to MreC *in vitro*¹⁴, the effect we observe is probably the result of reduced interaction with MreC. Taken together, our results indicate that the pedestal domain is important for proper function of the cell elongation machinery formed by RodA–PBP2 and its partners both *in vitro* and *in vivo*.

In addition to the extensive interactions between RodA and the PBP2 pedestal domain, a second surprising feature of the structure is the compact architecture of the complex, which extends only approximately 45 Å above the membrane plane (Fig. 3b,c). The peptidoglycan layer lies approximately 120 Å above the inner membrane in Gram-negative bacteria¹, raising the question of how the bBPB can reach the existing peptidoglycan mesh to crosslink newly synthesized glycan strands to it. Since the relative orientations of RodA and PBP2 could be influenced by crystal packing effects (Extended Data Fig. 8), we used negative-stain electron microscopy to investigate the complex in the absence of crystallographic constraints. The resulting two-dimensional (2D) class averages indicate that the RodA–PBP2 complex can adopt a range of conformations, including compact configurations like that seen in the crystal structure as well as more open, extended conformations (Fig. 3b and Extended Data Fig. 9). In the extended conformation, PBP2 may be able to reach approximately 100 Å above the membrane plane, positioning its active site near the existing peptidoglycan layer.

Genetic and biochemical studies on SEDS and bBPBs have suggested that these two proteins form a functional synthase that can both polymerize and crosslink peptidoglycan to form the bacterial cell wall^{1–5,11,20,21}. The RodA–PBP2 crystal structure and negative-stain electron microscopy analysis now provide molecular views of this complex, showing how SEDS proteins and bBPBs work together. In bacteria, this complex must be tightly regulated since inactivation of PBPs by β -lactams and/or of SEDS peptidoglycan activity leads to uncrosslinked glycan strands that result in a toxic cycle of peptidoglycan synthesis and degradation in Gram-negative bacteria¹⁸. Our data define the bBPB pedestal domain as a central

allosteric hub that regulates and coordinates peptidoglycan polymerization and crosslinking activities (Fig. 3c). By adopting both extended and compact conformations, we suggest that the bBPB can either promote peptidoglycan polymerization via allosteric modulation of RodA or favour the crosslinking of newly synthesized peptidoglycan by positioning the transpeptidase domain in proximity to the existing cell wall. The equilibrium between extended and compact conformations may be influenced by MreC or other proteins in the elongosome complex. Although its exact role remains incompletely defined, MreC probably serves as an additional regulator that structurally communicates with other Rod system proteins including MreD, RodZ and the cytoskeletal protein MreB, to ensure that peptidoglycan synthesis occurs only at the right time and location during the growth of rod-shaped bacterial cells. Future work is necessary to decipher additional layers of regulation that allow tight spatio-temporal control of peptidoglycan synthesis. The structure of the RodA–PBP2 complex provides a molecular view of how such regulation can be achieved and will facilitate detailed understanding of peptidoglycan synthesis and its regulation.

Methods

Protein expression and purification. The expression plasmids for *T. thermophilus* RodA and PBP2 (pMS235, pMS239, pMS292, pMS293 and pMS294) were transformed into the *E. coli* C43 derivative of BL21(DE3) harbouring an arabinose-inducible ubiquitin-like-specific protease 1 protease plasmid (pAM174) under the selection for both plasmids. Ten fresh transformants from each were inoculated into 5 ml Terrific Broth medium supplemented with 35 $\mu\text{g ml}^{-1}$ chloramphenicol and 50 $\mu\text{g ml}^{-1}$ kanamycin and allowed to grow overnight at 37 °C in a rolling shaker. The 5 ml overnight culture was then diluted in 1 l of Terrific Broth supplemented with 0.1% glucose, 2 mM of MgCl_2 , 50 $\mu\text{g ml}^{-1}$ of kanamycin and 35 $\mu\text{g ml}^{-1}$ of chloramphenicol. Cultures were grown at 37 °C until an OD₆₀₀ of 0.6 and allowed to cool down to 20 °C. At an OD₆₀₀ of approximately 0.8, protein expression was induced by adding isopropyl β -D-1-thiogalactopyranoside (IPTG, 1 mM final) and arabinose (0.2% final) for PBP2/RodA and ubiquitin-like-specific protease 1, respectively. After a 16 h induction, cells were collected and frozen at –80 °C. The same procedure was performed for ³⁵RodA alone (pMS211) except that 100 $\mu\text{g ml}^{-1}$ of ampicillin was used instead of kanamycin. Expression of the *E. coli* RodA–PBP2 complex was performed using the same method, except that expression was carried out using the CAM333 strain of the *E. coli* C43 derivative of BL21(DE3) (ref. 1).

Cells were thawed and resuspended in lysis buffer (50 mM of HEPES, pH 7.5, 150 mM of NaCl, 20 mM of MgCl_2 , 1:100,000 (v/v) benzonase nuclease), lysed by sonication, and membranes were collected by ultracentrifugation at 50,000g for 1 h at 4 °C. Co-expressed FLAG-3C-RodA and PBP2-3C-PrC were extracted using a glass dounce tissue grinder (DWK Life Sciences) in a solubilization buffer containing 20 mM of HEPES, pH 7.5, 500 mM of NaCl, 20% (v/v) glycerol and 1% (w/v) *n*-Dodecyl β -D-maltoside (DDM; Anatrace). Samples were stirred for 2 h at 4 °C, then centrifuged as before for 1 h. The supernatant containing solubilized FLAG-3C-RodA and PBP2-3C-PrC was supplemented with 2 mM of CaCl₂ and loaded by gravity flow onto 5 ml anti-FLAG antibody affinity resin. The resin was washed extensively with 20 \times column volumes of buffer containing 20 mM of HEPES, pH 7.0, 500 mM of NaCl, 20% glycerol and 0.1% DDM. The protein complex was eluted by adding 5 mM of EDTA and 0.2 mg ml⁻¹ FLAG peptide. PBP2-PrC was co-eluted with FLAG-RodA as analysed by SDS–polyacrylamide gel electrophoresis (PAGE). A similar procedure was performed for RodA in isolation (pMS211). For the purification of PBP2 in isolation (pMS235), the same procedure was performed except that the solubilized fraction was loaded onto 6 ml anti-protein C antibody affinity resin, pre-equilibrated with 20 mM of HEPES, pH 7.0, 500 mM of NaCl, 20% glycerol and 0.1% DDM, washed as stated earlier and then eluted by adding 5 mM of EDTA and 0.2 mg ml⁻¹ protein C peptide. Each sample was further purified by size-exclusion chromatography (SEC) on a Sephadex S200 column (GE Healthcare) in buffer containing 20 mM of HEPES, pH 7.5, 500 mM of NaCl and 0.1% DDM. After preparatory SEC, proteins to be subjected to the crystallization trials were concentrated to 40–60 mg ml⁻¹ using a Vivaspin 20 MWCO 100 Centrifugal Concentrator with a 100 kDa molecular weight cut-off (Vivaproducts) and flash-frozen with liquid nitrogen in aliquots of 8 μl . For the enzymatic assays and electron microscopy experiments, proteins were frozen at 1–2 mg ml⁻¹ and flash-frozen with liquid nitrogen in aliquots of 2 μl . Samples were stored at –80 °C until use for crystallography, electron microscopy or enzymatic assays. The purity and monodispersity of each sample were evaluated by SDS–PAGE and analytical SEC, respectively.

Expression of histidine-tagged *Enterococcus faecalis* PBP2X was performed as stated earlier and purification was performed as described previously²². Briefly, cells were collected by centrifugation and the pellet suspended in 50 ml of lysis buffer (20 mM of Tris, pH 7.5, 20 mM of MgCl_2 , 400 mM of NaCl) supplemented

with 1 mM of phenylmethylsulfonyl fluoride and 1:100,000 (v:v) benzonase nuclease. Cells were lysed by sonication and the cell lysate was pelleted by centrifugation at 50,000g for 45 min at 4°C. The resulting supernatant was supplemented with 10 mM of imidazole, added to 3 ml of Ni Sepharose Excel resin (GE Healthcare) equilibrated with 20 mM of Tris, pH 7.5, 400 mM of NaCl and 10 mM of imidazole. After loading the gravity column, the resin was washed with 20× column volumes wash buffer (20 mM of Tris, pH 7.5, 400 mM of NaCl, 20 mM of imidazole). The protein was eluted in 20 ml of elution buffer (20 mM of Tris, pH 7.5, 400 mM of NaCl, 200 mM of imidazole), concentrated to approximately 2 ml and dialysed against 4 l of 20 mM Tris, pH 7.5, and 400 mM of NaCl overnight at 4°C. Purity was evaluated by SDS-PAGE and the protein was aliquoted, flash-frozen in liquid nitrogen and stored at -80°C.

Crystallography and data collection. Purified *T. thermophilus* WT RodA-PBP2 and RodA^{D255A}-PBP2 complexes where tags had not been removed were diluted to a concentration of 35 mg ml⁻¹ and reconstituted into lipidic cubic phase by mixing monoolein (Hampton Research) using the coupled syringe reconstitution method²³. All samples were mixed at least 100 times before dispensing. The resulting phase was dispensed in 30–40 nl drops onto a glass plate and overlaid with 650 nl of precipitant solution using a Gryphon LCP robot (Art Robbins Instruments). Crystals for the WT RodA-PBP2 complex grew in precipitant solution containing 40–50% polyethylene glycol (PEG) 300 (Hampton Research), 100 mM lithium sulfate and 100 mM of 2-(*N*-morpholino)ethanesulfonic acid (MES) buffer, pH 5.7–6.4. The RodA^{D255A}-PBP2 complex was incubated with 5 mM of ampicillin for 1 h on ice before reconstitution and crystals grew in precipitant solution containing 35–45% PEG 300, 100 mM of sodium sulfate, 100 mM MES buffer, pH 5.8–6.8 and 10 mM of strontium chloride. Initial crystallization hits grew within 24 h, with diffraction-quality crystals reaching full size over the course of 1–4 weeks. Crystals were collected using mesh loops and stored in liquid nitrogen until data collection. Data collection was carried out at the Advanced Photon Source GM/CA beamline 23ID-B and 23ID-D. An initial grid raster with 80 × 30 μm² beam dimensions was performed to locate crystals within the loop. Additional fine-tuning rasters were performed using a 10 μm beam diameter to optimize the position of the crystal for data collection. Data were collected using a 10 μm beam and 0.2° oscillation per frame at a wavelength of 1.033 Å and a fivefold attenuation factor for beamline 23ID-B and no attenuation for beamline 23ID-D. For the WT RodA-PBP2 and RodA^{D255A}-PBP2 complexes, a complete dataset was obtained from two and five crystals, respectively. Diffraction data were indexed and processed using the X-ray Detector Software (XDS, v.20190315)²⁴. Both the WT RodA-PBP2 and RodA^{D255A}-PBP2 complexes crystallized in the P3₂1 space group with 1 molecule in the asymmetric unit with a solvent content of approximately 75%.

Phasing and refinement. The structure of *T. thermophilus* RodA (PDB code: 6BAR) was used as a single search template for molecular replacement in Phaser v.2.8.0 (ref. 25). The top scoring solution (as judged by both TF-Z and LLG metrics) was used as a fixed partial solution for a second round of molecular replacement that used the transpeptidase domain (residues Ala137–Leu487) of *Mycobacterium tuberculosis* PBPA²⁶ (PDB code: 3LO7) as a search model for PBP2. The final model was solved by manual building using Coot v.0.8.9.2-pre-revision-7884 (ref. 27) and reciprocal space refinement using phenix.refine v.1.16-3549 (ref. 28). The RodA-PBP2 crystals for both WT and D255A variant displayed diffraction anisotropy. For the D255A dataset, 2 of the 3 principal axes diffracted to 3.3 Å; the other diffracted to 2.8 Å. For the WT dataset, two axes diffracted to 3.5 Å and the other diffracted to 3.1 Å. The Diffraction Anisotropy Server²⁹ was used to perform ellipsoidal truncation, followed by anisotropic scaling and isotropic B-factor correction. Attempts were made to use the corrected structure factors during initial model building; however, the electron density maps were of similar quality compared to the non-scaled datasets, so we chose to use the original dataset (that is, without ellipsoidal truncation) during refinement.

Verification of the sequence register for the transmembrane portion of PBP2 was straightforward and unambiguous due to the frequency of bulky amino acid side chains and the available evolutionary coupling data¹¹. The 2Fo–Fc electron density map is shown in Extended Data Fig. 10. The structure of the RodA^{D255A}-PBP2 complex was solved using the WT RodA-PBP2 complex as the molecular replacement search model and the resulting refined structure was nearly identical to that of WT RodA (0.13 Å RMSD between all Cα atoms). In both WT and D255A datasets, an ambiguous density was observed between the anchor and head region of the pedestal domain of PBP2. This region was modelled as a poly-alanine peptide and may reflect a trace amount of MreC or a different peptide fragment from *E. coli* that copurified with the complex. The B-factors for the complex were the lowest in the transpeptidase domain of PBP2 and at the interface between the transmembrane portion of PBP2 and the TM8 and TM9 of RodA. The highest B-factors were observed for the TM7 and ECL4 of RodA. After refinement, the quality of both structures was assessed using MolProbity v.4.02-528 (ref. 30) to calculate Ramachandran statistics and other parameters. In the WT RodA-PBP2 structure, 93.7% of residues were in Ramachandran-favoured regions and 6.4% were in Ramachandran-allowed regions. For the RodA (D255A)-PBP2 structures, these values were 92.6% and 7.4%, respectively. No Ramachandran outliers

were present in either structure. Figures were prepared in PyMOL v.2.0 (<https://pymol.org/2/>). All crystallographic data processing, refinement and analysis software was compiled and supported by the SBGrid Consortium³¹. The sequence conservation analysis shown in Fig. 1f was computed using the ConSurf Server³². Briefly, a multiple sequence alignment of *T. thermophilus* RodA to 150 of its closest homologues was calculated using the HHMER algorithm provided by the ConSurf Server. A similar analysis was performed with *T. thermophilus* PBP2. The resulting ConSurf conservation scores were visualized with PyMOL. Conservation scores were divided into nine equally sized categories of conservation ranging from slowly evolving (that is, conserved) to rapidly evolving (that is, variable) sites. The colouring reflects the relative degree of conservation of each amino acid position.

Electron microscopy. For negative staining, 2.5 μl of protein solution consisting of RodA-PBP2 complex at a concentration of 0.005 mg ml⁻¹ in 0.01% DDM (w/v) was added to a glow-discharged, carbon-coated copper grid (Electron Microscopy Sciences) and allowed to adsorb for 30 s. Grids were then washed twice with deionized water and stained twice with freshly prepared 1.5% (w/v) uranyl formate. Filter paper was applied to the grid to absorb residual liquid between each step. Samples were then allowed to dry for approximately 2 min. Images used to generate the 2D classes shown in Fig. 3 were collected at room temperature using a Philips Tecnai T12 electron microscope equipped with a lanthanum hexaboride filament and operated at 120 kV. Images were collected at a magnification of 67,000-fold, corresponding to a pixel size of 1.68 Å, and a defocus value of -1.5 μm on a Gatan 4K charge-coupled device camera using a low-dose collection procedure. Approximately 1,000 particles were manually picked in RELION (REGularized Likelihood OptimizatioN, v.3.0.7_cu9.0)³³; then, an auto-picking routine picked the remaining particles for a total of 32,152. 2D class averages were calculated with RELION. Similar class averages were observed when calculated with EMAN2 v.2.22, 2.21a_sge, 2.21a and 2.07 (ref. 34).

Glycosyltransferase activity assay. To assess enzymatic activity, the lipid II substrate was purified from *E. faecalis* as described previously²². Peptidoglycan polymerization reactions were adapted from previously described methods^{5,22,35}. Briefly, 1 μM of purified *T. thermophilus* RodA-PBP2 complex or variants thereof were incubated with 20 μM of lipid II in reaction buffer containing 50 mM of Tris, pH 7.5, 20 μM of MnCl₂ and 30% dimethylsulfoxide. All proteins were purified in 0.1% DDM; therefore, the working concentration of DDM in the assay was 0.02%. All reactions were incubated at 25°C for 5–30 min and quenched by incubation at 98°C for 5 min. Peptidoglycan biotinylation of each reaction mixture was performed by adding biotinylated D-lysine (2 mM, working concentration) and purified *E. faecalis* PBP2X (10 μM, working concentration) followed by incubation at 25°C for 30 min. The biotinylation reaction was then quenched by adding 11 μl 2× SDS loading dye. The samples were then loaded into a 4–20% gradient polyacrylamide gel and run at 180 V for 35 min. The products were transferred onto a polyvinylidene fluoride membrane (Bio-Rad Laboratories) and fixed in 0.4% paraformaldehyde diluted in PBS for 30 min at room temperature. The membrane was blocked with SuperBlock (TBS) blocking buffer (Thermo Fisher Scientific) for 1 h at room temperature and the biotinylated products were detected by incubation with fluorescently tagged streptavidin (IRDye 800CW streptavidin, 1:5,000 in SuperBlock; LI-COR Biosciences) for an additional 1 h at room temperature. Membranes were washed three times for 10 min each with tris-buffered saline and Polysorbate 20 (0.01% Tween 20) and then twice for 10 min each in PBS. Blots were visualized with an Odyssey CLx imaging system (LI-COR Biosciences).

***E. coli* strain construction.** All plasmids were initially transformed into TB28 chemically competent cells and plated on lysogeny broth medium supplemented with 25 μg ml⁻¹ chloramphenicol. The *pbpA-rodA::aph* mutation was then introduced by P1-mediated transduction, using FB38(ΔFB190)/pFB194 (ref. 36) as a donor. Transductants were selected on M9 minimal medium³⁷ supplemented with 0.2% casamino acids, 0.2% glucose and 50 μg ml⁻¹ of kanamycin.

***E. coli* spot titres.** Overnight cultures of cells deleted for the *pbpA-rodA* locus (FB38), harbouring vectors producing the indicated alleles of *pbp-rodA* from a pLac-regulated plasmid (pRY47, pHC857, pPRI48, pPRI151, pPRI152 and pPRI190) were serially diluted and spotted on either M9 agar supplemented with 0.2% casamino acids and 0.2% glucose, lysogeny broth agar containing 100 μM of IPTG or lysogeny broth agar containing 100 μM of IPTG and 10 mM of DTT. Plates were incubated at 30°C for 16 h (lysogeny broth) or 40 h (M9).

Microscopy. Overnight cultures of these strains were diluted to an OD₆₀₀ of 0.05 in 3 ml of M9 medium supplemented with 0.2% casamino acids, 0.2% maltose and 25 μM of IPTG. Cells were grown at 30°C until the OD₆₀₀ reached 0.2, at which point cells were spotted onto filter discs placed on lysogeny broth agar medium supplemented with 100 μM of IPTG, with or without 10 mM of DTT. After 6 h growth at 30°C, cells were suspended in liquid lysogeny broth medium, fixed and imaged using phase contrast microscopy (scale bar, 5 μm). Where indicated, cells were fixed in 2.6% formaldehyde with 0.04% glutaraldehyde at room temperature for 1 h, followed by storage at 4°C for 24 h. Before imaging, cells were immobilized on 2% agarose pads and covered with no. 1.5 coverslips.

Imaging was performed on a Nikon Ti inverted microscope equipped with a 100× Plan apochromat 1.4 numerical aperture phase contrast objective, Zyla 4.2 sCMOS camera (Andor) and Nikon motorized stage. The acquisition software was the NIS-Elements imaging software v.4.30. Purchase of this microscope was funded in part by grant no. S10 RR027344-01. Microscopy was performed with the support of the Microscopy Resources on the North Quad (MicRoN) facility at Harvard Medical School. The ImageJ plug-in MicrobeJ v.5.13k³⁸ was used to segment cells and measure cell dimensions. Statistical significance was determined using a two-way analysis of variance followed by Tukey's multiple comparison test.

Plasmid construction. The pMS235 (*ColA-P₁₇-TiPBP2-3C-PrtC*) plasmid was generated in a two-piece isothermal assembly reaction with *TiPBP2-3C-PrtC* (amplified from *T. thermophilus* PBP2 gBlock (Integrated DNA Technologies) using primers oMS235f (5'-ATTTTGTCTAACTTAATAAGGAGATATACCATGGGTACAGGCCCGCATCCAGCC-3') and oMS235r (5'-GCATTATGCGCCGCAAGCTTTTATTGTCCATCAATCAGCG-3')) and pCOLADuet-1 (Novagen) digested with NcoI and HindIII.

The pMS239 (*ColA-P₁₇-TiPBP2-3C-PrtC; P₁₇-His6-SUMO-Flag-3C-TiRodA*) plasmid was generated in a two-piece isothermal assembly reaction with *His6-SUMO-Flag-3C-TiRodA* (amplified from pMS211) using the oligonucleotide primers oMS239f (5'-CACGGATGCTGACGTCGGTACCTCGAGATGCGTGTTTCTCACCAC-3') and oMS239r (5'-GTTATTGCTCAGCGGTGGCAGCAGCTAGGTAGTCTTGGTAGCGGTCACGATGCAAG-3') and pMS235 digested with XhoI and AvrII.

The pMS244 (*ColA-P₁₇-TiPBP2-3C-PrtC; P₁₇-His6-SUMO-Flag-3C-TiRodA* (D255A)) plasmid was generated by site-directed mutagenesis on pMS239.

The pMS292 (*ColA-P₁₇-TiPBP2-3C-PrtC; P₁₇-His6-SUMO-Flag-3C-TiRodA* (L43R)) plasmid was generated by site-directed mutagenesis on pMS239.

The pMS293 (*ColA-P₁₇-TiPBP2-3C-PrtC; P₁₇-His6-SUMO-Flag-3C-TiRodA* (A186R)) plasmid was generated by site-directed mutagenesis on pMS239.

The pMS294 (*ColA-P₁₇-TiPBP2-3C-PrtC; P₁₇-His6-SUMO-Flag-3C-TiRodA* (R149-GS-E162)) plasmid was generated in a three-piece isothermal assembly reaction with PBP2 fragment 1 (amplified from pMS239 using the oligonucleotide primers oMS235f and oMS294r (5'-CCTCTCAGATCCACGTAATACGTATCCATAACAGGCC-3')) and PBP2 fragment 2 (amplified from pMS239 with oMS294bf (5'-CGTATTACGTGGATCTGAAGAGGAAGTGGGCCAGG-3') and oMS235r) and pMS239 digested with NcoI and HindIII.

For the pPR148 (*colE1 cat lacI^q P_{lac}::pbpA(A147C)-rodA*) plasmid, the QuikChange method (Stratagene) of site-directed mutagenesis was performed to introduce the *pbpA(A147C)* substitution into template pHC857 (ref. ¹⁸), using primer o147QC (5'-GACCGAAGTACAAGTAGCTCGCTTTGCGTCAATCA-GTACCGTTTTCCGGGTGTCGAAG-3').

For the pPR151 (*colE1 cat lacI^q P_{lac}::pbpA(R237C)-rodA*) plasmid, the QuikChange method of site-directed mutagenesis was performed to introduce the *pbpA(R237C)* substitution into the pHC857 (ref. ¹⁸) template using primer o237QC (5'-GTAAACAACCGTGGCGTGTATTGGCCAGTAAAAGAAGTACCACCGCAAG-3').

For the pPR152 (*colE1 cat lacI^q P_{lac}::pbpA(A147C/R237C)-rodA*) plasmid, the o761 (5'-CCCGCGAAATTAATACGACTCACTATAGGG-3'), o147C_R (5'-CTGATTGACGAAAAGCGAGCTACTTGTACTTCGG-3'), o147C_QC (5'-GACCGAAGTACAAGTAGCTCGCTTTGCGTCAATCAGTACCGTTTTCCGGGTGTCGAAG-3') and o1320 (5'-TAAATGGTCCCTCCGTCGG-3') primers were used to introduce the A147C substitution into the pPR151 (*pbpA-R237C*) template using overlap extension PCR. The product was PCR-purified, digested with XbaI/KpnI and cloned into similarly digested pHC857 (ref. ¹⁸).

For the pPR190 (*colE1 cat lacI^q P_{lac}::pbpA(L61R/A147C/R237C)-rodA*) plasmid, a 5' fragment of the *pbpA(L61R)* gene was amplified from the genomic DNA of a *pbpA(L61R)* mutant strain⁹, using primers o761 (5'-CCCGCGAAATTAATACGACTCACTATAGGG-3') and o147C_R (5'-CTGATTGACGAAAAGCGAGCTACTTGTACTTCGG-3'). A 3' fragment of *pbpA(A147C/R237C)* was amplified from pPR152 using the primers o147C_QC (5'-GACCGAAGTACAAGTAGCTCGCTTTGCGTCAATCAGTACCGTTTTCCGGGTGTCGAAG-3') and o1320 (5'-TAAATGGTCCCTCCGTCGG-3'). Overlap extension PCR was then performed to combine and amplify these two fragments using primers o761 and o1320. The resulting product was PCR-purified, digested with XbaI/KpnI and cloned into similarly digested pHC857 (ref. ¹⁸).

Reporting Summary. Further information on research design is available in the Nature Research Reporting Summary linked to this article.

Data availability

Structure factors and refined atomic coordinates for the WT RodA–PBP2 complex and RodA(D255A)–PBP2 variant complex have been deposited in the RCSB PDB under accession codes 6PL5 and 6PL6, respectively. All other data that support the findings of this study are available from the corresponding author upon request. The source data for Figs. 2b and 2d are provided with the paper.

Received: 12 August 2019; Accepted: 11 February 2020;

Published online: 09 March 2020

References

- Meeske, A. J. et al. SEDS proteins are a widespread family of bacterial cell wall polymerases. *Nature* **537**, 634–638 (2016).
- Emami, K. et al. RodA as the missing glycosyltransferase in *Bacillus subtilis* and antibiotic discovery for the peptidoglycan polymerase pathway. *Nat. Microbiol.* **2**, 16253 (2017).
- Cho, H. et al. Bacterial cell wall biogenesis is mediated by SEDS and PBP polymerase families functioning semi-autonomously. *Nat. Microbiol.* **1**, 16172 (2016).
- Rohs, P. D. A. et al. A central role for PBP2 in the activation of peptidoglycan polymerization by the bacterial cell elongation machinery. *PLoS Genet.* **14**, e1007726 (2018).
- Taguchi, A. et al. FtsW is a peptidoglycan polymerase that is functional only in complex with its cognate penicillin-binding protein. *Nat. Microbiol.* **4**, 587–594 (2019).
- Reichmann, N. T. et al. SEDS–bPBP pairs direct lateral and septal peptidoglycan synthesis in *Staphylococcus aureus*. *Nat. Microbiol.* **4**, 1368–1377 (2019).
- Silhavy, T. J., Kahne, D. & Walker, S. The bacterial cell envelope. *Cold Spring Harb. Perspect. Biol.* **2**, a000414 (2010).
- Scheffers, D.-J. & Tol, M. B. LipidII: just another brick in the wall? *PLoS Pathog.* **11**, e1005213 (2015).
- Otten, C., Brilli, M., Vollmer, W., Viollier, P. H. & Salje, J. Peptidoglycan in obligate intracellular bacteria. *Mol. Microbiol.* **107**, 142–163 (2018).
- Ruiz, N. Lipid flippases for bacterial peptidoglycan biosynthesis. *Lipid Insights* **8**, 21–31 (2016).
- Sjodt, M. et al. Structure of the peptidoglycan polymerase RodA resolved by evolutionary coupling analysis. *Nature* **556**, 118–121 (2018).
- Caffrey, M. A comprehensive review of the lipid cubic phase or in meso method for crystallizing membrane and soluble proteins and complexes. *Acta Crystallogr. F Struct. Biol. Commun.* **71**, 3–18 (2015).
- Levy, N. et al. Structural basis for *E. coli* penicillin binding protein (PBP) 2 inhibition, a platform for drug design. *J. Med. Chem.* **62**, 4742–4754 (2019).
- Contreras-Martel, C. et al. Molecular architecture of the PBP2–MreC core bacterial cell wall synthesis complex. *Nat. Commun.* **8**, 776 (2017).
- Mravic, M. et al. Packing of apolar side chains enables accurate design of highly stable membrane proteins. *Science* **363**, 1418–1423 (2019).
- Ovchinnikov, S., Kamisetty, H. & Baker, D. Robust and accurate prediction of residue–residue interactions across protein interfaces using evolutionary information. *eLife* **3**, e02030 (2014).
- Hopf, T. A. et al. Sequence co-evolution gives 3D contacts and structures of protein complexes. *eLife* **3**, e03430 (2014).
- Cho, H., Uehara, T. & Bernhardt, T. G. Beta-lactam antibiotics induce a lethal malfunctioning of the bacterial cell wall synthesis machinery. *Cell* **159**, 1300–1311 (2014).
- Otero, L. H. et al. How allosteric control of *Staphylococcus aureus* penicillin binding protein 2a enables methicillin resistance and physiological function. *Proc. Natl Acad. Sci. USA* **110**, 16808–16813 (2013).
- Fay, A., Meyer, P. & Dworkin, J. Interactions between late-acting proteins required for peptidoglycan synthesis during sporulation. *J. Mol. Biol.* **399**, 547–561 (2010).
- Fraipont, C. et al. The integral membrane FtsW protein and peptidoglycan synthase PBP3 form a subcomplex in *Escherichia coli*. *Microbiology* **157**, 251–259 (2011).
- Welsh, M. A. et al. Identification of a functionally unique family of penicillin-binding proteins. *J. Am. Chem. Soc.* **139**, 17727–17730 (2017).
- Caffrey, M. & Cherezov, V. Crystallizing membrane proteins using lipidic mesophases. *Nat. Protoc.* **4**, 706–731 (2009).
- Kabsch, W. XDS. *Acta Crystallogr. D Biol. Crystallogr.* **66**, 125–132 (2010).
- McCoy, A. J. et al. Phaser crystallographic software. *J. Appl. Crystallogr.* **40**, 658–674 (2007).
- Fedarovich, A., Nicholas, R. A. & Davies, C. Unusual conformation of the SxN motif in the crystal structure of penicillin-binding protein A from *Mycobacterium tuberculosis*. *J. Mol. Biol.* **398**, 54–65 (2010).
- Emsley, P. & Cowtan, K. Coot: model-building tools for molecular graphics. *Acta Crystallogr. D Biol. Crystallogr.* **60**, 2126–2132 (2004).
- Afonine, P. V. et al. Towards automated crystallographic structure refinement with phenix.refine. *Acta Crystallogr. D Biol. Crystallogr.* **68**, 352–367 (2012).
- Strong, M. et al. Toward the structural genomics of complexes: crystal structure of a PE/PPE protein complex from *Mycobacterium tuberculosis*. *Proc. Natl Acad. Sci. USA* **103**, 8060–8065 (2006).
- Chen, V. B. et al. MolProbity: all-atom structure validation for macromolecular crystallography. *Acta Crystallogr. D Biol. Crystallogr.* **66**, 12–21 (2010).
- Morin, A. et al. Collaboration gets the most out of software. *eLife* **2**, e01456 (2013).

32. Ashkenazy, H. et al. ConSurf 2016: an improved methodology to estimate and visualize evolutionary conservation in macromolecules. *Nucleic Acids Res.* **44**, W344–W350 (2016).
33. Scheres, S. H. W. RELION: implementation of a Bayesian approach to cryo-EM structure determination. *J. Struct. Biol.* **180**, 519–530 (2012).
34. Tang, G. et al. EMAN2: an extensible image processing suite for electron microscopy. *J. Struct. Biol.* **157**, 38–46 (2007).
35. Qiao, Y. et al. Detection of lipid-linked peptidoglycan precursors by exploiting an unexpected transpeptidase reaction. *J. Am. Chem. Soc.* **136**, 14678–14681 (2014).
36. Bendezú, F. O. & de Boer, P. A. J. Conditional lethality, division defects, membrane involution, and endocytosis in Mre and Mrd shape mutants of *Escherichia coli*. *J. Bacteriol.* **190**, 1792–1811 (2008).
37. Smale, S. T. β -galactosidase assay. *Cold Spring Harb. Protoc.* **2010**, pdb.prot5423 (2010).
38. Ducret, A., Quardokus, E. M. & Brun, Y. V. MicrobeJ, a tool for high throughput bacterial cell detection and quantitative analysis. *Nat. Microbiol.* **1**, 16077 (2016).

Acknowledgements

Financial support for the work was provided by National Institutes of Health grant nos. U19AI109764 (A.C.K., D.Z.R., T.G.B., S.W. and D.K.), R01GM106303 (D.S.M.) and 5F31GM128233-02 (S.C.E), the Howard Hughes Medical Institute (T.G.B.) and a Canadian Institutes of Health Research doctoral research award to P.D.A.R. We thank the Advanced Photon Source GM/CA beamline staff for the excellent facilities and technical assistance during X-ray data collection and M. Welsh for the generous gift of purified lipid II substrate.

Author contributions

M.S. performed the large-scale purification and crystallization of the RodA–PBP2 complexes, the enzymatic assays and negative-stain electron microscopy and data processing. S.C.E. collected the electron microscopy images and provided input on data processing. M.S.A.G. assisted with revisions and performed small-scale protein purification. A.T., D.K. and S.W. provided additional input regarding the enzyme assays. M.S., S.Z. and A.C.K. solved and refined the structure. K.B. and A.G.G., with supervision by D.S.M., performed additional validation of the RodA–PBP2 structure using evolutionary couplings. P.D.A.R. assessed the PBP2 mutant phenotypes with supervision from T.G.B. and D.Z.R. A.C.K. performed the overall project supervision with input from T.G.B. and D.Z.R. M.S. and A.C.K. wrote the manuscript with input from the other authors.

Competing interests

The authors declare no competing interests.

Additional information

Extended data is available for this paper at <https://doi.org/10.1038/s41564-020-0687-z>.

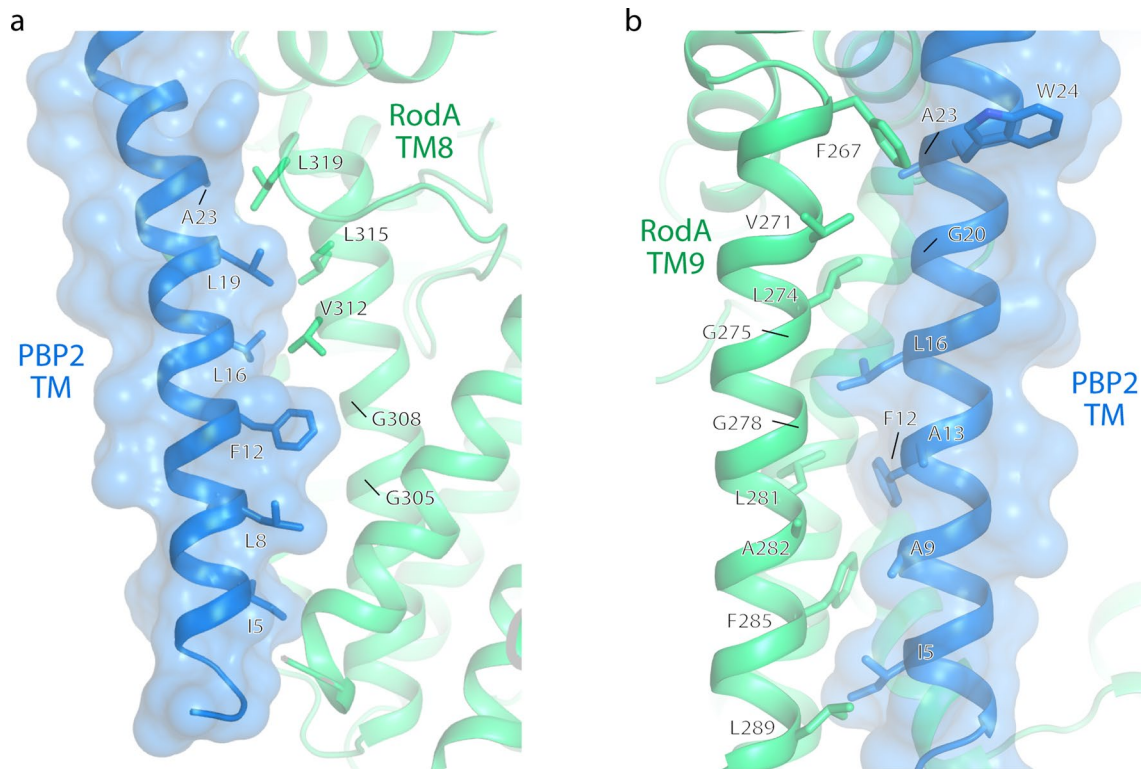
Supplementary information is available for this paper at <https://doi.org/10.1038/s41564-020-0687-z>.

Correspondence and requests for materials should be addressed to A.C.K.

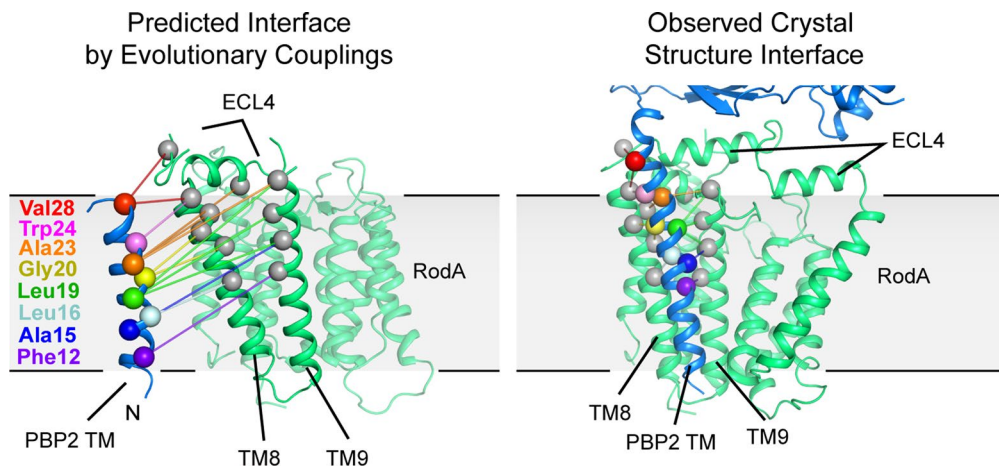
Reprints and permissions information is available at www.nature.com/reprints.

Publisher's note Springer Nature remains neutral with regard to jurisdictional claims in published maps and institutional affiliations.

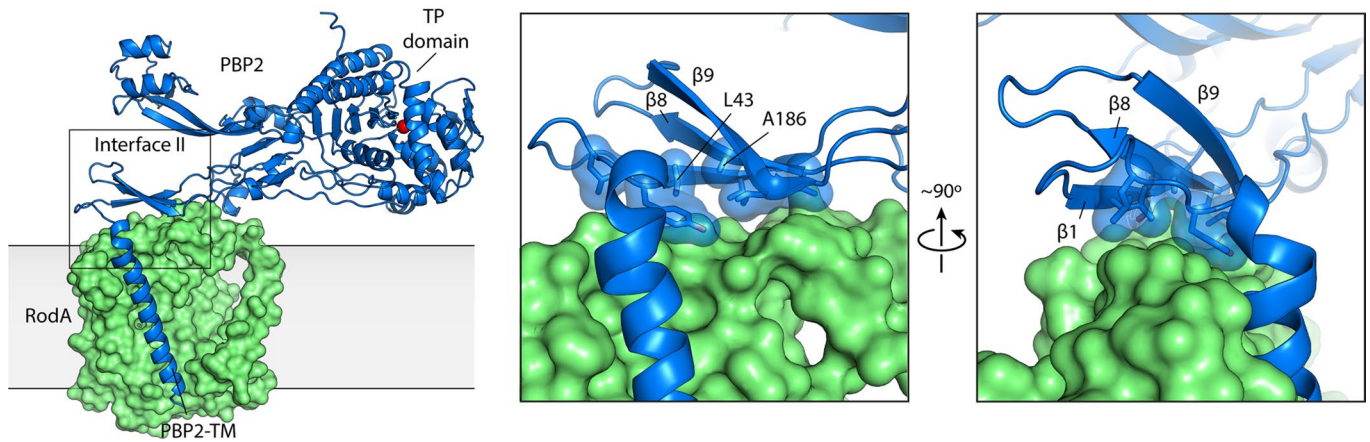
© The Author(s), under exclusive licence to Springer Nature Limited 2020



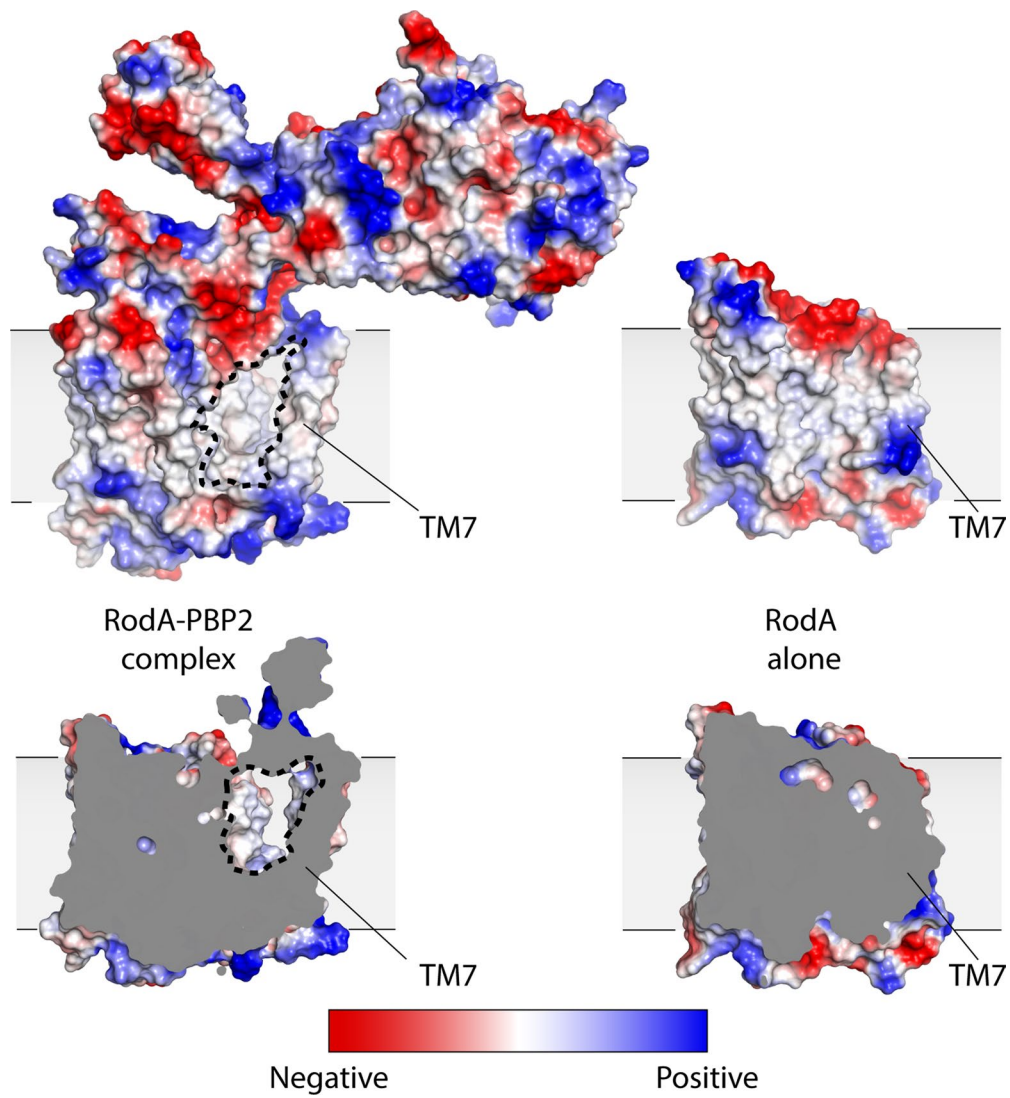
Extended Data Fig. 1 | RodA-PBP2 complex interface within the membrane plane. The transmembrane helix of PBP2 is shown as blue ribbons and transparent molecular surfaces to highlight its interaction with **a**, RodA transmembrane helix 8 and **b**, RodA transmembrane helix 9.



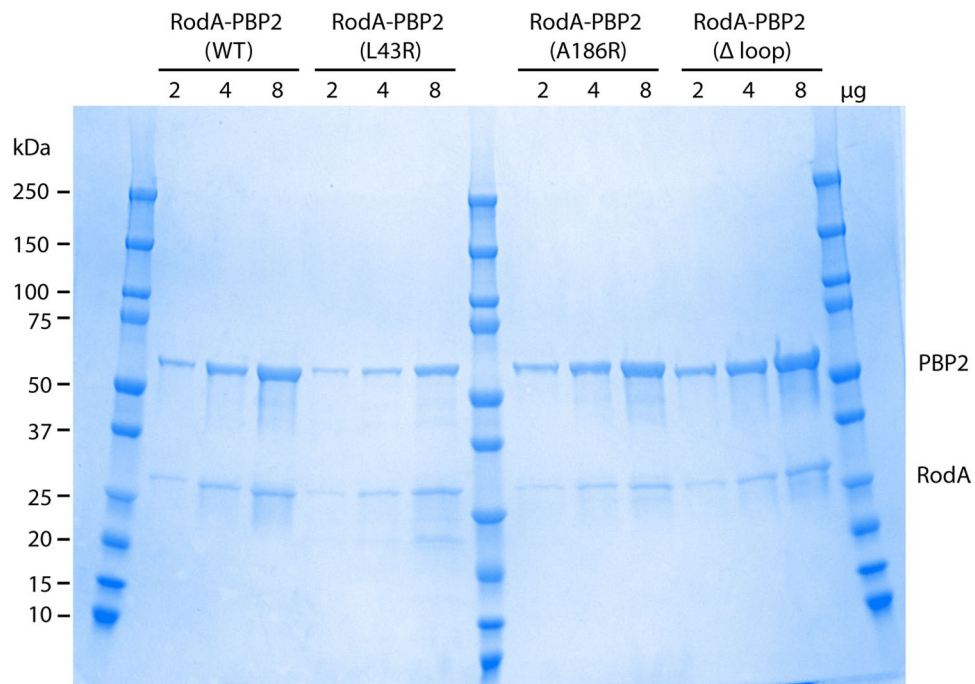
Extended Data Fig. 2 | Evolutionary covariation analysis of RodA-PBP2 interface. Graphical representation of 19 evolutionary couplings between RodA-PBP2.



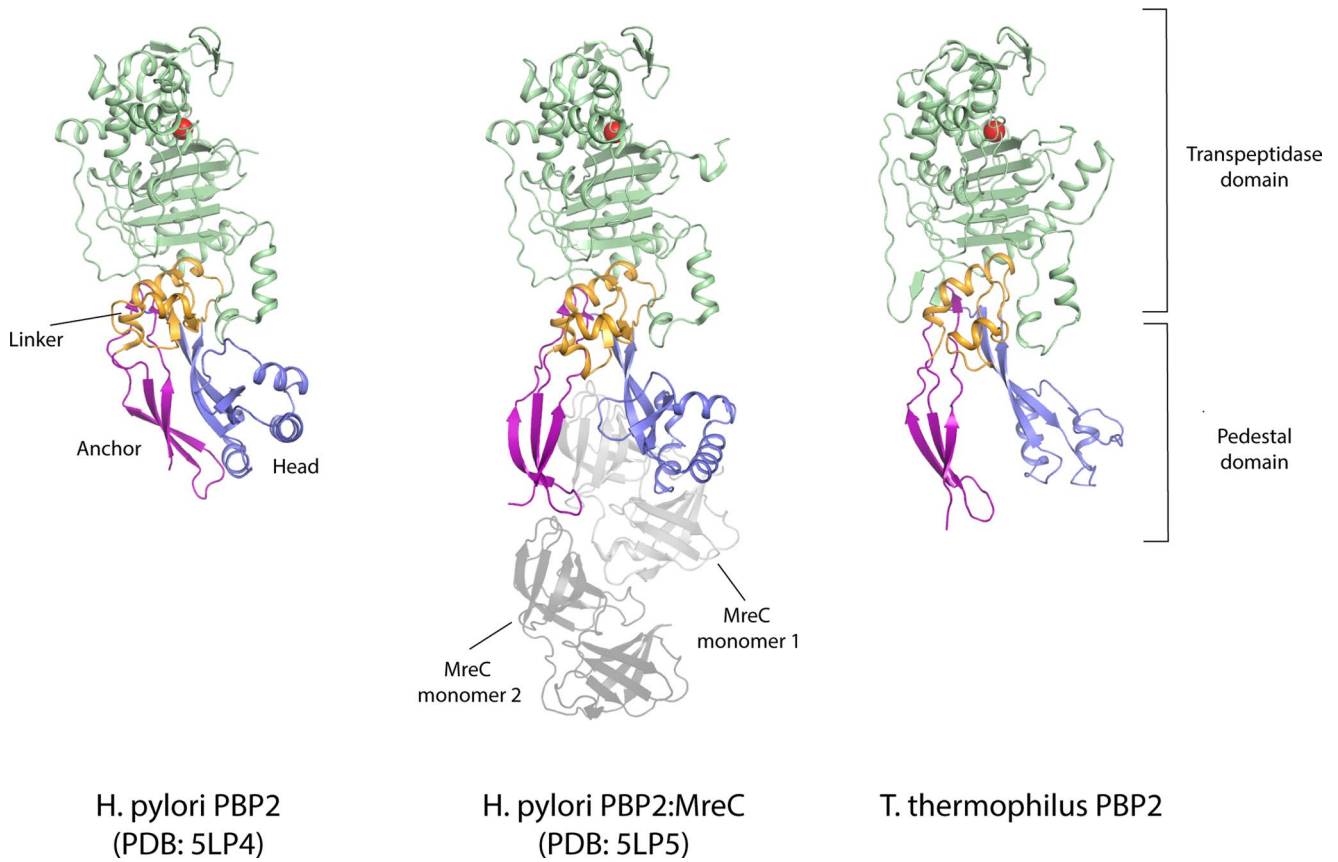
Extended Data Fig. 3 | RodA-PBP2 complex interface II. PBP2 is shown as ribbons colored blue and RodA is shown as molecular surfaces and colored green. The insets show two views of interface II. Side chains of PBP2 residues at the RodA interface are shown as sticks with hydrophobic residues also shown as transparent molecular surface to highlight surface complementarity. Two PBP2 residues that disrupted RodA function when substituted with arginine are labeled.



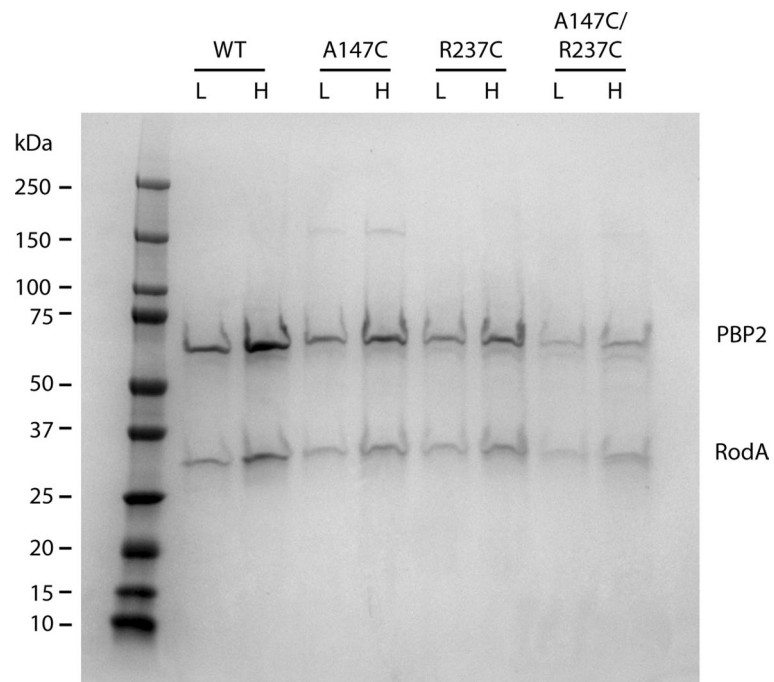
Extended Data Fig. 4 | Shift of TM7 of RodA in complex with PBP2 results in a large membrane-accessible cavity. Surface view of RodA:PBP2 complex (left) and RodA (right) representing electrostatic potential (top panel) and a cross section (bottom panel). The large surface-exposed cavity is outlined in black dotted lines.



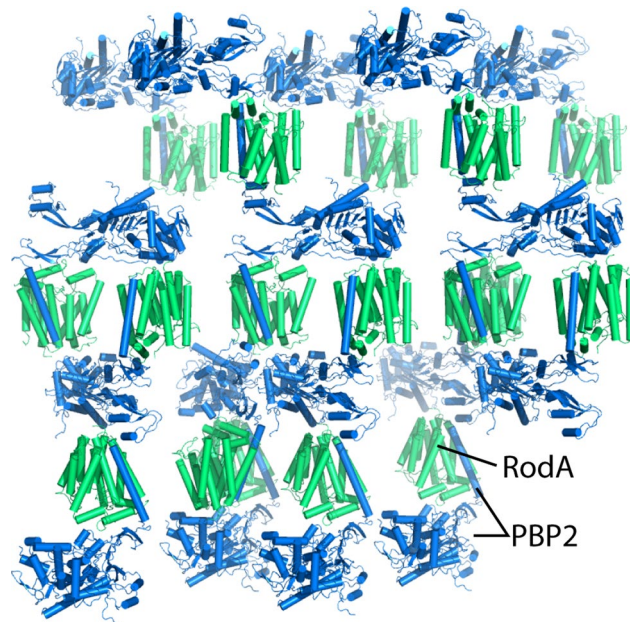
Extended Data Fig. 5 | PBP2 mutants co-purify with RodA. PBP2 variants were co-expressed with FLAG-tagged RodA and purified using anti-FLAG affinity resin. SDS-PAGE gel showing the elution from the anti-FLAG affinity resin demonstrates that PBP2 remains associated with RodA throughout the purification. Results are derived from one experiment.



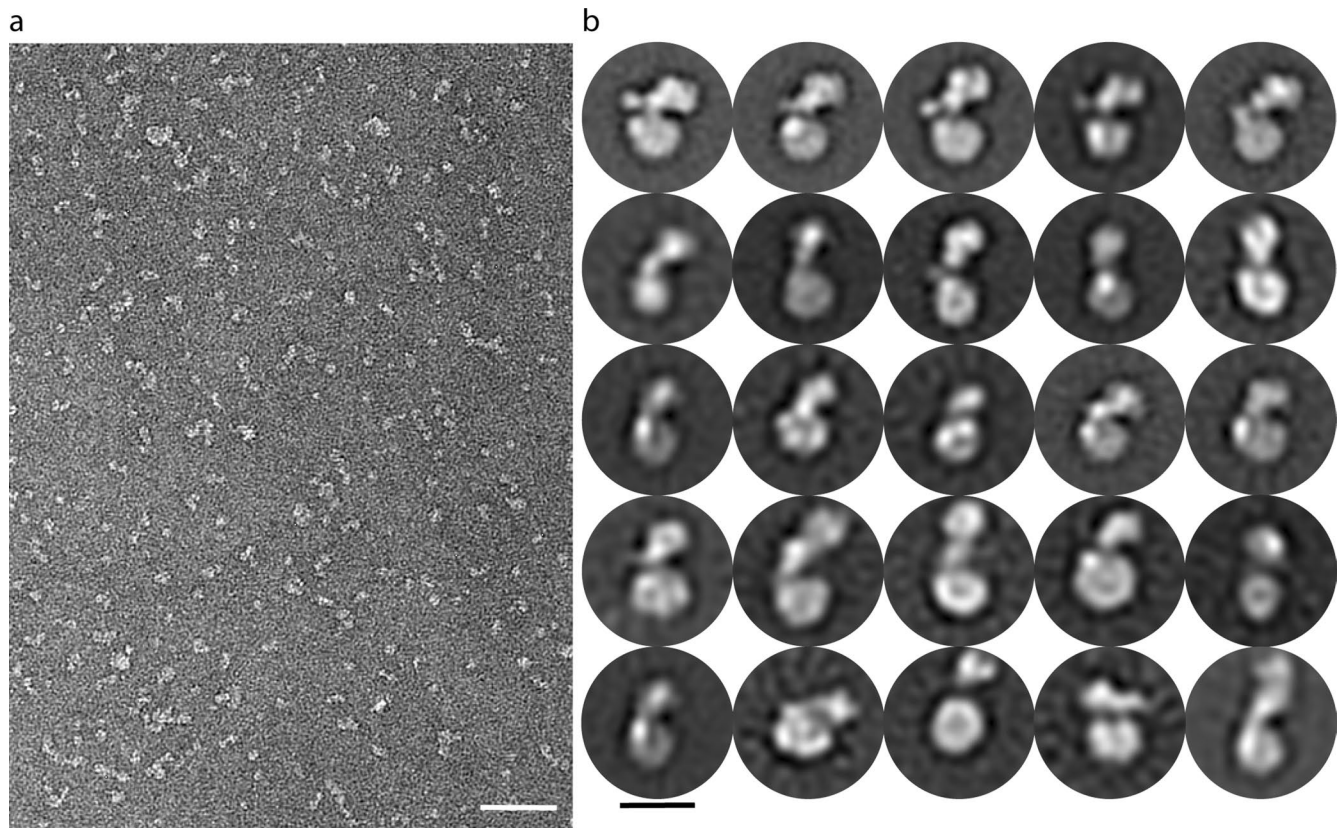
Extended Data Fig. 6 | Structural comparison of extracytoplasmic domains of PBP2 from *T. thermophilus* and *H. pylori*. The catalytic serine in each transpeptidase is shown as a red sphere.



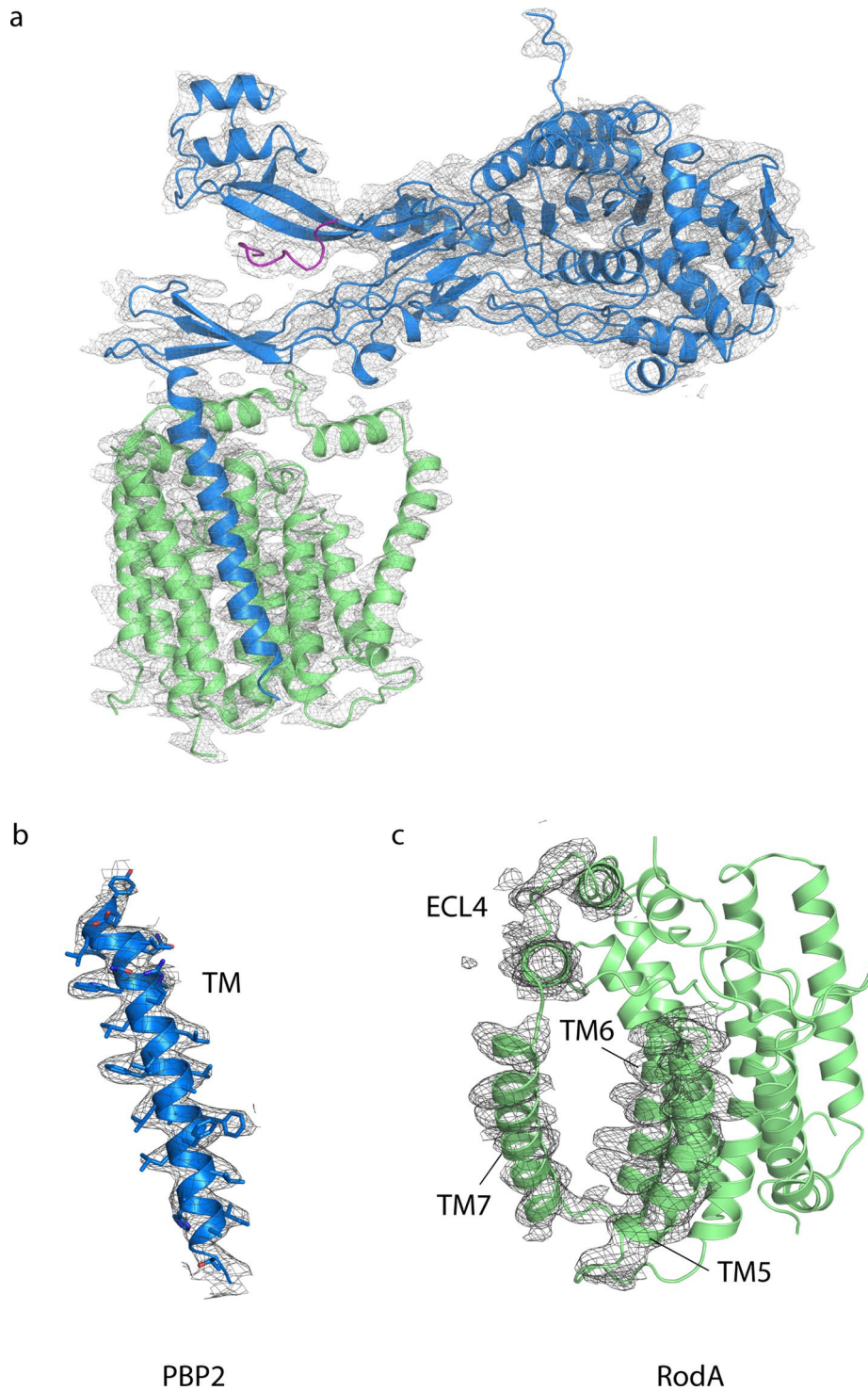
Extended Data Fig. 7 | *E. coli* PBP2 variants co-purify with *E. coli* RodA. PBP2 variants were co-expressed with FLAG-tagged RodA and purified using anti-FLAG affinity resin. SDS-PAGE gel showing the elution from the anti-FLAG affinity resin demonstrates that PBP2 remains associated with RodA throughout the purification. Low (L) and high (H) correspond to approximately 2 μ g and 4 μ g as measured by A_{280} . Results are derived from one experiment.



Extended Data Fig. 8 | RodA-PBP2 complex crystal lattice. The ^{13}C RodA:PBP2 complex adopts type 1 lipid cubic phase crystal packing. RodA and PBP2 are shown in green and blue, respectively.



Extended Data Fig. 9 | EM analysis of ^{13}C RodA-PBP2 complex. **a**, Representative EM micrograph of negatively stained RodA:PBP2 complex solubilized in DDM detergent micelles. Scale bar denotes 50 nm. **b**, Representative two-dimensional class averages from a total of 32,152 particles. Scale bar represents 10 nm. Results are derived from one experiment.



Extended Data Fig. 10 | Electron density map. $2F_o - F_c$ electron density map contoured at 1.0σ within a 2.3 \AA radius of atoms shown for **a**, the entire *T. thermophilus* RodA:PBP2 complex **b**, the transmembrane helix of PBP2 and **c**, transmembrane helices 5–7 and extracellular loop 4 of RodA.

Reporting Summary

Nature Research wishes to improve the reproducibility of the work that we publish. This form provides structure for consistency and transparency in reporting. For further information on Nature Research policies, see [Authors & Referees](#) and the [Editorial Policy Checklist](#).

Statistics

For all statistical analyses, confirm that the following items are present in the figure legend, table legend, main text, or Methods section.

n/a Confirmed

- The exact sample size (n) for each experimental group/condition, given as a discrete number and unit of measurement
- A statement on whether measurements were taken from distinct samples or whether the same sample was measured repeatedly
- The statistical test(s) used AND whether they are one- or two-sided
Only common tests should be described solely by name; describe more complex techniques in the Methods section.
- A description of all covariates tested
- A description of any assumptions or corrections, such as tests of normality and adjustment for multiple comparisons
- A full description of the statistical parameters including central tendency (e.g. means) or other basic estimates (e.g. regression coefficient) AND variation (e.g. standard deviation) or associated estimates of uncertainty (e.g. confidence intervals)
- For null hypothesis testing, the test statistic (e.g. F , t , r) with confidence intervals, effect sizes, degrees of freedom and P value noted
Give P values as exact values whenever suitable.
- For Bayesian analysis, information on the choice of priors and Markov chain Monte Carlo settings
- For hierarchical and complex designs, identification of the appropriate level for tests and full reporting of outcomes
- Estimates of effect sizes (e.g. Cohen's d , Pearson's r), indicating how they were calculated

Our web collection on [statistics for biologists](#) contains articles on many of the points above.

Software and code

Policy information about [availability of computer code](#)

Data collection

JBlulce Data Acquisition Software for Macromolecular Crystallography, Version 201x.y, Digital micrograph version 3.94 for Gatan Microscopy Suite version 1.4.4, NIS Elements 4.30

Data analysis

ADXV version 1.9.14, XDS version 20190315, Phenix version 1.16-3549, Coot version 0.8.9.2-pre-revision-7884, Molprobity version 4.02-528, Relion 3.0 version 3.0.7_cu9.0, EMAN2 version 2.22, 2.21a_sge, 2.21a, 2.07, ImageJ 1.52q, MicrobeJ 5.13k

For manuscripts utilizing custom algorithms or software that are central to the research but not yet described in published literature, software must be made available to editors/reviewers. We strongly encourage code deposition in a community repository (e.g. GitHub). See the Nature Research [guidelines for submitting code & software](#) for further information.

Data

Policy information about [availability of data](#)

All manuscripts must include a [data availability statement](#). This statement should provide the following information, where applicable:

- Accession codes, unique identifiers, or web links for publicly available datasets
- A list of figures that have associated raw data
- A description of any restrictions on data availability

Structure factors and refined atomic coordinates for wild type RodA:PBP2 complex and the RodA(D255A):PBP2 mutant complex are deposited in the RCSB Protein Data Bank under accession codes 6PL5 and 6PL6, respectively.

Field-specific reporting

Please select the one below that is the best fit for your research. If you are not sure, read the appropriate sections before making your selection.

Life sciences Behavioural & social sciences Ecological, evolutionary & environmental sciences

For a reference copy of the document with all sections, see [nature.com/documents/nr-reporting-summary-flat.pdf](https://www.nature.com/documents/nr-reporting-summary-flat.pdf)

Life sciences study design

All studies must disclose on these points even when the disclosure is negative.

Sample size	Sample sizes are indicated in figure legends.
Data exclusions	No data were excluded
Replication	All data shown are representative of multiple independent experiments, all attempts at replication have been successful.
Randomization	Randomization was not used since no prospective treatments were performed in this work.
Blinding	No blinding was used. Blinding during collection of X-ray diffraction data and other data types presented here is not standard practice and is unlikely to affect results or their interpretation.

Reporting for specific materials, systems and methods

We require information from authors about some types of materials, experimental systems and methods used in many studies. Here, indicate whether each material, system or method listed is relevant to your study. If you are not sure if a list item applies to your research, read the appropriate section before selecting a response.

Materials & experimental systems

n/a	Involvement in the study
<input checked="" type="checkbox"/>	<input type="checkbox"/> Antibodies
<input checked="" type="checkbox"/>	<input type="checkbox"/> Eukaryotic cell lines
<input checked="" type="checkbox"/>	<input type="checkbox"/> Palaeontology
<input checked="" type="checkbox"/>	<input type="checkbox"/> Animals and other organisms
<input checked="" type="checkbox"/>	<input type="checkbox"/> Human research participants
<input checked="" type="checkbox"/>	<input type="checkbox"/> Clinical data

Methods

n/a	Involvement in the study
<input checked="" type="checkbox"/>	<input type="checkbox"/> ChIP-seq
<input checked="" type="checkbox"/>	<input type="checkbox"/> Flow cytometry
<input checked="" type="checkbox"/>	<input type="checkbox"/> MRI-based neuroimaging